12-1-2016

Direct Quadrature Method of Moments with Delumping for Modeling Multicomponent Droplet Vaporization

Simcha L. Singer
Marquette University, simcha.singer@marquette.edu

Accepted version. *International Journal of Heat and Mass Transfer,* Vol. 103 (December 2016): 940-954. DOI.

Direct Quadrature Method of Moments with Delumping for Modeling Multicomponent Droplet Vaporization

Simcha L. Singer

Department of Mechanical Engineering, Marquette University, Milwaukee, WI

Abstract

A multicomponent droplet vaporization model which combines the computational efficiency of continuous thermodynamic approaches with the detailed species information provided by discrete component models has been developed. The Direct Quadrature Method of Moments (DQMoM) is used to efficiently solve for the evolution of the nodes and weights of the equivalent liquid-phase mole fraction distribution without assuming any functional form. The novelty of the approach is an inexpensive delumping procedure that is used to reconstruct the time-dependent mole fractions and fluxes for all discrete species. When applied to a vaporizing kerosene droplet, agreement between the full discrete component model, which solves ODEs for every individual species, and DQMoM with delumping, which solves only a few ODEs, is excellent. This computationally inexpensive model is well-suited for implementation in CFD codes with detailed kinetic mechanisms, as it enables

[International Journal of Heat and Mass Transfer, Vol 103 (December 2016): pg. 940-954. DOI.

accurate calculation of species source terms from the droplets without incurring an unrealistic computational cost.

Keywords: Multicomponent droplet vaporization, Delumping, Continuous thermodynamics, Quadrature Method of Moments (QMoM), Direct Quadrature Method of Moments (DQMoM)

Nomenclature

A	group of variables in Eq. (30)
a	recursion coefficient in Eq. (13)
b	recursion coefficient in Eq. (13)
B_M	Spalding mass transfer number
B_T	Spalding heat transfer number
C	concentration, or group of variables in Eq. (30)
c_p	specific heat capacity
D	diffusion coefficient, or group of variables in Eq. (30)
E	group of variables in Eq. (30)
f	function multiplying weight function in Eq. (11)
I	distribution variable
J	integral in Eq. (38)
k	thermal conductivity
l_v	latent heat of vaporization
MW	molecular weight (molar mass)
m	moment
N	number of nodes
Nu	Nusselt number (based on droplet diameter)
$\dot{n}$	molar flow rate
n	number of discrete species
P	pressure
P_N	polynomial in Eq. (13)
p	integrand in Eq. (38)
R	radius of droplet
Re	Reynolds number (based on droplet diameter and slip velocity)
R_f	radius of gas film in modified Sherwood number
S	source term in CTM species equation
$\bar{S}$	source term in moment transformed species equation
Sc	Schmidt number
Sh	Sherwood number (based on droplet diameter)
T	temperature
t	time
u	integrating factor
w	weight
x	mole fraction
δ	delta function
ρ	density

Superscripts	
$*$	modified (Sherwood number, Nusselt number)
crit	critical
i	discrete species index
k	moment order index
tot	total (for all species or nodes)
Subscripts	
g	gas
i	discrete species index
j	node index
l	liquid
nb	normal boiling
ref	reference value for gas-phase calculated using 1/3 rule
s	at droplet surface
sat	Saturation
v	vapor (as in $c_{p,v}$ and l_v)
∞	at far-field boundary

1. Introduction

Vaporization of multicomponent liquid droplets occurs in a variety of engineering devices, such as engines and turbines. Such applications are often analyzed using computational fluid dynamics (CFD), with the behavior of the individual liquid droplets incorporated as a sub-model. Given the computational expense associated with CFD simulations, it is important that sub-models for droplet vaporization remain computationally inexpensive. At the same time, vaporization models that fail to provide information on the vaporization behavior of individual species reduce the accuracy of CFD simulations and may preclude the use of detailed chemical kinetic mechanisms that account for a large number of species.

Discrete component models (DCM) employ either ordinary differential equations (ODEs) or partial differential equations (PDEs) for each individual species within a vaporizing multicomponent droplet.[1,2] Given that common fuels typically consist of hundreds of components, this highly accurate approach is also the most computationally expensive, and in practice, cannot be applied to every species. To reduce computational cost, quasi-discrete models represent the mixture using a reduced number of quasi-components, each representing a range of species in terms of carbon number.[3] This

approach can be extended to include several different groups of molecules, each divided into quasi-components.[4] The quasi-components are then treated as discrete species in a multicomponent vaporization model. Surrogate mixture approaches, which attempt to replicate the vaporization (and/or combustion) behavior of complex fuels with several strategically chosen components[1,5] can also be considered a type of quasi-discrete approach.

In contrast to discrete approaches, continuous thermodynamic models (CTM) treat the composition of the multicomponent mixture as a continuous distribution function, often of molecular weight or normal boiling point.[6] Rather than solving PDEs/ODEs for every single species, classical CTM solve equations for the evolution of a distribution function of an assumed functional form, such as a gamma distribution.[7,8] However, assuming a specific functional form for the species distribution can lead to inaccuracies, especially as the distribution evolves in time. This prompted Laurent et al. to apply the Quadrature Method of Moments (QMoM) to droplet vaporization,[9] following the idea of Lage, who was the first to apply QMoM to a continuous mole fraction distribution, for the purpose of modeling flash vaporization.[10]

Similar to the original Method of Moments,[11] QMoM applies a moment transform to the species evolution equations and solves for the first k moments of the evolving distribution.[12] To deal with the closure problem – the appearance of moments of order higher than k in the evolution equations – QMoM employs a Gaussian quadrature approximation to express the unclosed integral terms as a function of moments order k and lower.[12] The Gaussian quadrature is written in terms of N weights and nodes, the latter corresponding to the roots of the polynomial of order N that is orthogonal to the weight function (the distribution function).[13] The product-difference algorithm[14] is often used as part of the procedure to determine the nodes at every time, although in some cases the product-difference algorithm can become unstable,[15] particularly as the order of the quadrature approximations increases.[16]

The Direct Quadrature Method of Moments (DQMoM) is an alternative approach that does not require the product-difference algorithm, or an analogue, at every time step.[17] DQMoM directly solves

evolution equations for an equivalent distribution function consisting of a summation of delta function with positions (nodes) and heights (weights) identical to the nodes and weights of the Gaussian quadrature approximation used in QMoM.[17] For univariate distributions, QMoM and DQMoM yield equivalent results, but DQMoM does not require the potentially unstable product-difference algorithm.[17]

The distillation curve method is a simpler implementation of a CTM approach. The distillation curve method accounts for multicomponent vaporization by varying a single progress variable, the mean molecular weight of the droplet, during vaporization, in accordance with data derived from distillation curves of various fuels.[18] In general, all CTM approaches reduce computational expense compared to DCM approaches, but information on the behavior of individual species is lost.

In addition to the question of how to represent the many chemical components present in liquid fuel droplets (DCM vs. CTM), a second issue that often arises is the treatment of temperature and species gradients within the droplets in a computationally efficient manner. Approaches range from assumptions of negligible internal temperature[19] and species gradients,[1,9,20] to analytical[8,21–23] or semi-analytical solutions[23] for internal temperature and species profiles, to discretization of the droplet interior.[24,25] CPU requirements for models requiring internal discretization of the droplets likely render them impractical as sub-models for CFD simulations.

The approach presented in this paper is concerned only with efficiently representing the multicomponent nature of the droplets and is compatible with more than one method for representing temperature and species gradients within the droplet. However, as will be seen below, not every treatment of internal species gradients is compatible with the delumping procedure described in this paper.

The model presented in this paper combines the computational efficiency of continuous thermodynamic models with the detailed species information provided by discrete component models. The starting point for the model is the work on kerosene droplets by Laurent et al. using QMoM9,[20] and Bruyat et al. using DQMoM,[15] to efficiently solve for the evolution of the liquid-phase mole fraction

distribution without assuming any functional form. The critical insight of this paper is that it is possible to develop a delumping procedure that can be used to obtain the time-dependent mole fractions and fluxes for all individual species with excellent accuracy and minimal computational cost. The delumping approach is compatible with any CTM, including QMoM and DQMoM, though DQMoM is implemented here and the overall method is referred to as "DQMoM with delumping."

The DQMoM with delumping approach will be demonstrated using the modeling framework of Laurent and coworkers[9,15,20] for the vaporization of well-mixed kerosene droplets. It is emphasized, however, that DQMoM with delumping is not necessarily restricted to well-mixed droplets. In Section 2.1, the full discrete form of the model is outlined, followed by the QMoM and DQMoM versions of the same model in Section 2.2, following Laurent and coworkers.[9,15,20] The novelty of the approach is the delumping strategy presented in Section 2.3. Results for a kerosene droplet with 36 components[9,15,20] and for a hypothetical droplet with 200 components are presented in Section 3, followed by conclusions and prospects for future applications in Section 4.

2. Droplet vaporization model

2.1. Discrete component model

Laurent and coworkers[9,15,20] begin with a classical DCM description[7] for the multicomponent vaporization of a spherically symmetric droplet of radius R without internal concentration gradients. Incorporating the results of Abramzon and Sirignano[26] for the gas film using a single averaged diffusion coefficient, D_g, and Sherwood number, Sh_g, for all components, ODEs for the evolution of each discrete liquid mole fraction, ${x^i}_l$, are given by:[9,15,20]

$$(1) \qquad \frac{d{x^i}_l}{dt} = \frac{3n^{tot}}{4\pi R^3 C_l}\left({x^i}_l - \frac{{x^i}_{g,s}\,(1+B_M) - {x^i}_{g,\infty}}{B_M}\right)$$

The total molar flow rate of vapor is

$$(2) \qquad \dot{n}^{tot} = 2\pi R C_g D_g {Sh^*}_g \ln(1+B_M)$$

[International Journal of Heat and Mass Transfer, Vol 103 (December 2016): pg. 940-954. DOI.

The definition of all symbols is provided in the nomenclature. The non-dimensional modified Sherwood number, Sh^*_g, and Spalding mass transfer number in molar units, B_M, are given by

$$(3) \qquad Sh^*_g = \frac{2R_f}{R_f - R} = 2 + \frac{0.6 Re^{1/2} Sc^{1/3}}{(1+B_M)^{0.7} \frac{\ln(1+B_M)}{B_M}}$$

$$(4) \qquad B_M = \frac{x^{tot}_{g,s} - x^{tot}_{g,\infty}}{1 - x^{tot}_{g,s}}$$

It is noted that $x^i_{g_1 s}$, the gas-phase mole fractions at the droplet surface and $x^i_{g_1 \infty}$, the gas-phase mole fractions at the far-field boundary, do not sum to unity, since they exclude non-condensable species that do not appear in the liquid phase (e.g. N_2 and O_2).

In most droplet vaporization models, including the present model,[9,15,20] vapor–liquid equilibrium at the droplet surface is treated using Raoult's Law, assuming an ideal gas and ideal solution:

$$(5) \qquad x^i_{g,s} = x^i_l \frac{P^i_{sat}(T)}{P_\infty}$$

Combining Eqs. (1)–(3) and rearranging yields the final discrete governing ODEs for each liquid species (mole fraction):

$$(6) \qquad \frac{dx^i_l}{dt} = \frac{3 C_g D_g Sh^*_g}{2R^2 C_l} \ln(1 + B_M) \left(x^i_l - x^i_{g,s} + \frac{x^i_{g,\infty} - x^i_{g,s}}{B_M}\right.$$

Solving Eqs. (3)–(6) for every species present in a multicomponent droplet constitutes a discrete component method. The flux of each discrete vapor component from the droplet to the surrounding gas, n^i , can be shown to be

$$(7) \qquad n^i = n^{tot} \left(\frac{x^i_{g,s}(1+B_M) - x^i_{g,\infty}}{B_M}\right)$$

The governing differential equations, Eq. (6), are non-linear, due to the dependence of B_M , and potentially Sh^*_g, on x^i_l , via the vapor–liquid equilibrium relation at the droplet surface, Eq. (5).

2.2. Continuous thermodynamics model

To reduce the computation time, Laurent and coworkers employed either QMoM[9,20] or DQMoM.[15] Rather than solving Eq. (6) for every discrete species present in the droplet, the droplet composition is assumed to be a continuous function of the distribution variable, *I*. In this case, *I* was chosen as the normal boiling point, T_{nb}. Both QMoM and DQMoM begin with a continuous version of Eq. (6), without assuming a functional form for the distribution of the liquid phase mole fraction, $x_l(I)$, which is free to evolve into any shape

$$\frac{dx_l(I)}{dt} = S(I,t) \tag{8}$$

The source term, $S(I, t)$, on the right-hand side, is

$$S(I,t) = \frac{3C_g D_g Sh^* g}{2R^2 C_l} \ln(1+B_M)\,(x_l(I) - x_{g,s}(I) + \frac{x_{g,\infty}(I) - x_{g,s}(I)}{B_M}) \tag{9}$$

Thermo-physical properties, such as D_g, C_g, C_l and P_{sat}, for the continuous mixture are also functions of the distribution variable, *I*. For the test cases described in Section 3, the correlations for physical properties as a function of normal boiling point are identical to those used by Laurent et al.[20] and are described in Appendix A.

When a droplet is composed of species with very different properties, it is possible to treat each group of species (e.g. alkanes, alcohols, etc.) as its own distribution and apply a continuous thermodynamic approach to each group. In this way, the accuracy of property correlations and the properties of the groups as a whole could be improved. While this approach could be used with the method described in this paper, it is assumed here that kerosene can be modeled with sufficient accuracy using a single distribution with properties dependent on T_{nb}, similar to Laurent et al.[20]

2.2.1. Quadrature Method of Moments (QMoM)

QMoM applies a moment transformation to Eq. (8) by multiplying both sides by I^k, for $k = 0{:}2N-1$, and integrating with respect to *I*. This yields 2*N* ODEs for the moments, $m^k{}_l$,

(10) $\frac{dm^k{}_l}{dt} = \bar{S}_k = \int_0^\infty S(I) I^k \, dI$

The source terms in these *k* equations, $\bar{S}_k$, require a closure - a method for evaluating them without introducing additional unknowns. This will be accomplished using a Gaussian quadrature approximation to the integral that appears in Eq. (10).[12] For the terms requiring a closure, it is possible to factor the integrand into a product of the original distribution function, $x_l(I)$, and everything left over, *f*(*I*)

(11) $\bar{S}_k = \int_0^\infty S(I) I^k dI = \int_0^\infty x_l(I) f(I) dI$

In this integral, the original distribution, $x_l(I)$, serves as the weight function. The quadrature is accurate if *f*(*I*) is approximately polynomial.[13] The quadrature approximation is given by

(12) $\int_0^\infty x_l(I) f(I) dI \approx \sum_{j=1}^N w_j f(I_j)$

with weights, w_j, and nodes, I_j. The quadrature is exact if is a polynomial of order $2N - 1$ or lower. The nodes, I_j , of the Gaussian quadrature correspond to the roots of an *N*th order polynomial, $P_N(I)$, that is orthogonal with respect to the weight function, $x_l(I)$, on the interval $(0, \infty)$. Finding the roots of this polynomial is most often accomplished using a recursion relation for orthogonal polynomials,[13]

(13) $P - 1(I) = 0, P0(I) = 1 P_{j+1}(I) = \big(I - a_j\big) P_j(I) - b_j P_{j-1}(I), (13)\ j = 0,1,2 \ldots$

The r elation can be expressed in matrix form with the eigenvalues of the matrix corresponding to the roots of $P_N(I)$ and thus, the nodes, I_j , of the quadrature. The weights, w_j , are related to the first component of the eigenvector of the matrix.[13] However, applying this procedure requires the determination of the coefficients a_j and b_j from the orthogonality condition, which in turn is expressed in terms of the moments, $m^k{}_l$. The latter is accomplished with either the product-difference algorithm[14] or Wheeler's algorithm.[27] Wheeler's algorithm has better stability characteristics than the product-difference algorithm.[16]

2.2.2. Direct Quadrature Method of Moments (DQMoM)

DQMoM is a stable alternative to QMoM that solves directly for the weights and nodes of the quadrature approximation in Eq. (12) and is mathematically equivalent to QMoM for univariate distributions.[17] DQMoM recognizes that the Gaussian quadrature approximation, Eq. (12), is equivalent to assuming that the (liquid mole fraction) distribution consists of a summation of *N* delta function located at nodes (normal boiling points), I_j, and with weights (mole fractions), w_j,

(14) $x_l(I) = \sum_{j=1}^{N} w_j \delta(I - I_j)$

Substituting this distribution function, Eq. (14), into the governing Eq. (8) yields

(15) $\sum_{j=1}^{N} \frac{\partial}{\partial t}\left[w_j \delta\left(I - I_j\right)\right] = S(I,t)$

Using the product rule, the chain rule and some rearrangement, the following equation is obtained:[13]

(16) $\sum_{j=1}^{N} \frac{dw_j}{dt}\left[\delta\left(I - I_j\right) + I_j \delta'\left(I - I_j\right)\right] - \sum_{j=1}^{N} \frac{d(w_j I_j)}{dt}\left[\delta'\left(I - I_j\right)\right] = S(I,T)$

Applying a moment transformation by multiplying both sides of Eq. (16) by I^k for k = 0:2N − 1, integrating with respect to I from 0 to ∞, and using the rules

(17) $\int_0^\infty I^k \delta\left(I - I_j\right) dI = {I^k}_j$

(18) $\int_0^\infty I^k \delta'\left(I - I_j\right) dI = -k{I^{k-1}}_j$

one obtains 2N differential equations for ${d(w_j)}/{dt}$ and ${d(w_j I_j)}/{dt}$ that can be solved *directly* for the N time-dependent nodes, I_j , and N time-dependent weights, w_j , of the equivalent distribution $x_l(I)$:[13]

(19) $(1-k)\sum_{j=1}^{N} {I^k}_j \frac{dw_j}{dt} + k\sum_{j=1}^{N} {I^{k-1}}_j \frac{d(w_j I_j)}{dt} = \int_0^\infty S(I) I^k dI = \bar{S}_k,\ k = 0,1 \ldots 2N-1$

The source terms on the right-hand side, $\bar{S}_k$, contain integrals of Eq. (9) with respect to *I* that are evaluated using the quadrature approximations in Eq. (12), and thus depend on w_j and I_j. Eq. (19) represents a system of 2*N* ordinary differential equations and can be cast in matrix form as:[13]

(20)

$$\begin{bmatrix} 1 & \cdots & 1 & 0 & \cdots & 0 \\ 0 & \cdots & 0 & 1 & \cdots & 1 \\ -I^2{}_1 & \cdots & -I^2{}_N & 2I_1 & \cdots & 2I_N \\ \vdots & \vdots & \vdots & \vdots & \vdots & \vdots \\ 2(1-N)I^{2N-1}{}_1 & \cdots & 2(1-N)I^{2N-1}{}_N & (2N-1)I^{2N-2}{}_1 & \cdots & (2N-1)I^{2N}{}_N \end{bmatrix} \begin{bmatrix} dw_1/dt \\ \vdots \\ dw_N/dt \\ d(w_1I_1)/dt \\ \vdots \\ d(w_NI_N)/dt \end{bmatrix} = \begin{bmatrix} \bar{S}_0 \\ \vdots \\ \vdots \\ \vdots \\ \bar{S}_{2N-1} \end{bmatrix}$$

This system of nonlinear differential equations for $d(w_j)/dt$ and $d(w_jI_j)/dt$ are solved directly for the weights, and the nodes, I_j , of the Gaussian quadrature. The first row of Eq. (20) ensures that the weights sum to unity. For the CTM droplet vaporization model represented by Eqs. (8) and (9), the right-hand side source terms, $\bar{S}_k$, are given by

(21) $$\bar{S}_k = \frac{3}{2R^2} \int_0^\infty I^k \frac{C_g D_g Sh^* g}{C_l} \ln(1+B_M)\left(x_l(I) - x_{g,s}(I) + \frac{x_{g,\infty}(I) - x_{g,s}(I)}{B_M}\right) dI$$

In the CTM approach, the Spalding mass transfer number is given by

(22) $$B_M = \frac{\int_0^\infty x_l(I)\frac{P_{sat}(I)}{P_\infty} dI - \int_0^\infty x_{g,\infty}(I) dI}{1 - \int_0^\infty x_l(I)\frac{P_{sat}(I)}{P_\infty} dI}$$

Using Eq. (14), this becomes

$$(23)\ B_M = \frac{\int_0^\infty x_l(I)\frac{P_{sat}(I)}{P_\infty}dI - \int_0^\infty x_{g,\infty}(I)dI}{1-\int_0^\infty x_l(I)\frac{P_{sat}(I)}{P_\infty}dI}$$

It is noted that with respect to the moment transform integral in Eq. (21), B_M is a constant, since it is characteristic of the gas mixture as a whole and the integrals in Eq. (22) are evaluated prior to those in Eq. (21). Similarly, properties of the mixture as a whole, such as C_l, D_g, etc. are also evaluated with an inner integral and are constants with respect to the integration in Eq. (21). For example, for mixture properties that are calculated as weighted averages by mole fraction, such as the liquid concentration, the mixture liquid concentration is given by

$$(24)\ C_l = \int_0^\infty C_l(I)x_l(I)dI$$

substituting using Eq. (14) yields

$$(25)\ C_l = \int_0^\infty C_l(I)\sum_{j=1}^N w_j\delta\left[I - I_j\right]dI$$

$$(26)\ C_l = \sum_{j=1}^N w_j C_l(I_j)$$

which is subsequently used in Eq. (21). Using the correlations for kerosene properties as a function of normal boiling point and temperature results in

$$(27)\ C_l = \sum_{j=1}^N\left(A_0 + A_1 I_j + A_2 {I^2}_j\right)w_j + \sum_{j=1}^N(B_0 + B_1 I_j + B_2 {I^2}_j)\bar{T}_l w_j$$

where the correlation coefficients are from Laurent et al.[20] and can be found in Appendix A. Eq. (27) is identical to Eq. (A.15).

Therefore, applying Eq. (14) to the *k* source terms in Eq. (21) yields

$$(28)\ \bar{S}_k = \frac{3C}{2R^2}\ln(1+B_M)\left[\sum_{j=1}^N w_j {I^k}_j\left(1 - \frac{P_{sat}(I_j T_s)}{P_\infty}\right) - \sum_{j=1}^N w_j {I^k}_j\left(\frac{P_{sat}(I_j,T_s)}{P_\infty B_M}\right) + \sum_{i=1}^n {I^k}_i\frac{{x^i}_{g,\infty}}{B_M}\right]$$

where *C* is defined to group several properties characteristic of the mixture as a whole

[International Journal of Heat and Mass Transfer, Vol 103 (December 2016): pg. 940-954. DOI.

$$(29)\ C \equiv \frac{Sh^*_g C_g D_g}{C_l}$$

As mentioned above, these terms are constants with respect to the integral in Eq. (21).

It is also noted that in the present paper, the far-field boundary conditions for the gas species are assumed to be constant[15] and are not coupled to the droplet vaporization. Therefore, the last term containing $x^i_{g,\infty}$ is evaluated using the full known boundary conditions for every discrete species, i = 1:n, rather than j = 1:N.

Initial conditions for the weights and nodes can be calculated using a single application of the product-difference algorithm[14] or Wheeler's algorithm[27] at time t = 0. Wheeler's algorithm is employed in this study. As will be seen later and as shown by Bruyat et al.,[15] excellent results are typically obtained with N = 3 or 4. Because only 2N differential equations are solved for the species equations in DQMoM, for droplets consisting of tens to hundreds of components, considerable savings are obtained compared to Eq. (6), which is solved for every discrete component. However, like QMoM and all CTM approaches, only the behavior of the mixture as a whole is obtained using DQMoM and information on the behavior of individual species is lost.[9,15,20] The delumping procedure described below has been developed to address this shortcoming.

2.3. Delumping

The novelty of the current approach is a delumping procedure that can recover information on individual species with minimal computational cost, after applying a CTM approach, such as DQMoM or QMoM. While delumping procedures have been applied to CTM and quadrature methods governed by *algebraic* equations for flash tank calculations,[28,29] delumping procedures using CTM results have not been developed for phenomena governed by nonlinear *differential* equations.

The key idea behind the delumping procedure is that any first-order, linear ordinary differential equation, no matter how complex, has an exact solution that can be written in terms of integrals with

respect to the independent variable, which is time, *t*, in the case of Eq. (6). This is the well-known "integrating factor" method.[30] If the nonlinearity of the DCM differential equation appears exclusively in terms associated with the multicomponent mixture as whole, which is the case for Eq. (6), it is possible to substitute for those terms using a CTM solution (e.g. DQMoM). In this way, the nonlinear differential equation can be converted to a linear differential equation, which can then be integrated numerically to obtain the evolution of every discrete species. Computationally, numerical integration is a very inexpensive operation compared to the numerical solution of differential equations. Therefore, DQMoM with delumping provides information on every species at a much smaller cost than solving a discrete differential equation for every species.

In the case of multicomponent droplet vaporization, in examining DCM Eqs. (4)–(6), the primary source of nonlinearity in the governing differential equations (6) are the B_M terms and their dependence on ${x^i}_l$. However, B_M is associated with the mixture as a whole, since it depends on the *sum* of ${x^i}_{g,s}$. Therefore, DQMoM can be used to efficiently solve for the evolution of the distribution as a whole, by solving for w_j and I_j using Eq. (20), as well as B_M at all times using Eq. (23). A second source of nonlinearity in discrete Eq. (6), is the dependence of properties C_g, D_g and C_l on the *mixture* composition, ${x^i}_l$. Since these terms are also associated with the mixture as a whole, DQMoM (or any CTM) can be used to calculate them as well. The approximations of these time-dependent terms, calculated by DQMoM, are then substituted into discrete Eq. (6), which is thus converted into a first order *linear* differential equation, since B_M, C_g, D_g and C_l are no longer functions of ${x^i}_l$, but rather, known functions of time. It is noted that though other terms in Eq. (6) may vary with time, none contain a nonlinear dependence on ${x^i}_l$.

Discrete Eq. (6) is rewritten below, where terms B_M, A, C, D_i and E_i are time-dependent. Terms D_i and E_i are unique to each discrete species, i, whereas terms B_M, A and C are the same for each discrete species.

$$\text{(30)}\quad \frac{d{x^i}_l}{dt} = ACln(1+B_M)D_i + ACln(1+B_M)E_i{x^i}_l$$

$$\text{(31a)}\quad A = \frac{3}{2R^2}$$

[International Journal of Heat and Mass Transfer, Vol 103 (December 2016): pg. 940-954. DOI.

(31b) $C = \frac{Sh^*_g C_g D_g}{C_l}$

(31c) $D_i = \frac{x^i_{g,\infty}}{B_M}$

(31d) $E_i = 1 - \frac{P^i{}_{sat}(T)}{P_\infty} - \frac{P^i{}_{sat}(T)}{P_\infty B_M}$

The solution to Eq. (30) can be expressed analytically as a function of integrals with respect to time using the integrating factor method. The integrating factor, $u_i(t)$, is

(32) $u_i(t) = \exp[\int_0^t -A(t)C(t)\ln(1+B_M(t))E_i(t)dt]$

and the delumped solution for each individual species is given by

(33) $x^i{}_l(t) = \frac{\int_0^t u_i(t)A(t)C(t)\ln(1+B_M(t))D_i(t)dt + x^i{}_l(0)}{u_i(t)}$

after substituting the values of B_M, C_g, C_l and D_g calculated from DQMoM into discrete Eqs. (32) and (33). This delumping step is computationally inexpensive and yields the state variables $x^i{}_l(t)$ for every species. Equations (5) and (7) can then be used to obtain the gas mole fractions at the surface and the vapor flux, respectively, for every individual species. Because the delumping step is analytically exact, it is only limited by the accuracy of the numerical integration used for Eqs. (32) and (33). The factor limiting the accuracy of the overall approach, then, is the performance of the DQMoM (or whatever CTM is chosen) in calculating the evolution of the mixture as a whole.

It is noted that at later times the integrating factor, $u_i(t)$, may become very large for certain species, due to the exponential in Eq. (32). When this is the case, the delumped solution for such species given by Eq. (33) results in an indeterminate form (∞/∞). In such cases, L'Hôpital's rule may be used on Eq. (33) to obtain the delumped solution as

(34) $x^i{}_l(t) = -\frac{D_i(t)}{E_i(t)}$

This is identical to the solution that one would obtain from the governing differential equation by setting the derivative term in Eq. (30) to zero at long times.

For a droplet containing *n* discrete species, using the definition of B_M from Eq. (4), it can be shown that the sum of the *n* discrete governing Eqs. (6) is identically zero, $\sum_i {dx^i}_l/_{dt} = 0$. This implies that the sum of the mole fractions is unity, $\sum_i {x^i}_l = 1$, provided the initial mole fractions sum to unity. For DQMoM with delumping, however, since B_M is evaluated using the weights, the sum of the *n* discrete governing equations (6) used in the delumping step is no longer identically zero, though typically the deviation is quite small. To ensure that DQMoM with delumping yields discrete liquid phase mole fractions that sum to unity, the delumped mole fractions from Eqs. (33) or (34) can be normalized using

$$(35)\quad {x^i}_{l,normalized} = \frac{{x^i}_l}{\sum_i {x^i}_l}$$

Mole fractions reported in Section 3 have been normalized in this way.

2.4. Other submodels and properties

DQMoM with delumping can be applied to multicomponent droplet vaporization whenever the nonlinearity of the governing species equation appears solely in terms associated with the mixture as a whole, as it is in Eq. (6). As long as this condition holds for the species equations, the equations used to determine the evolution of the droplet temperature and radius do not affect the applicability of delumping. For instance, the droplet temperature can be assumed to be uniform, quasi-steady and parabolic,[22] or can be calculated from more complex effective conductivity models.[23] For the results presented in Section 3, a parabolic temperature profile model was employed.[22] This leads to an ODE for the evolution of mean liquid temperature, $\bar{T}_l$ coupled with a nonlinear algebraic equation for the evolution of the droplet surface temperature, $T_{l,s}$.[31] The latter temperature is used in calculating the vapor–liquid equilibrium, while the former is used in calculating temperature-dependent liquid properties. Equations governing the evolution of the droplet temperature are given in Appendix B. For simplicity, in the results presented, it was assumed that the modified Sherwood and Nusselt numbers are identical. Furthermore, the modified Sherwood number in Eq. (3) is evaluated by simply prescribing R_f = 50 cm, which results in

$Sh_g^* \approx 2$ rather than including the correlation and its dependence on Reynolds, Schmidt and Spalding numbers. This implies that the droplet is almost completely entrained in the surrounding flow with negligible slip velocity. This is not a requirement for application of DQMoM with delumping, but was implemented for simplicity in demonstration of the approach.

The radius of the droplet evolves according to the classical ordinary differential equation representing conservation of mass across the liquid–vapor interface[26] and is given in Appendix B. This equation reduces to the d^2 law if the vaporization rate from the droplet is constant in time.

Thermo-physical properties for kerosene components as functions of the distribution variable, I, which is normal boiling point, T_{nb}, are given by correlations[20,32] and are provided in Appendix A. Mixing rules governing the behavior of the liquid and gas phases as a whole are identical to those used by Laurent et al.[20] and are also provided in Appendix A. Properties of the gas film are treated as uniform with position and calculated using the 1/3 rule. Relations between variables, such as between saturation pressure, P_{sat}, and liquid surface temperature, $T_{l,s.}$ are taken from Laurent et al. as well.[20]

2.5. Numerical implementation

Both DQMoM with delumping and the full DCM were coded in MATLAB and integrated using the differential–algebraic system solver IDA.[33] The system is one of differential–algebraic equations rather than differential equations due to the coupled nonlinear equation that is solved for the droplet surface temperature, $T_{l,s}$. The relative tolerance was set to 1×10^{-5} for both models. For DQMoM with delumping, the absolute tolerance for the weights, w_j and for the droplet radius, R, was set to 1×10^{-7}, while the absolute tolerance for the weights multiplied by the nodes, $w_j I_j$, and for the temperatures $\bar{T}_l$ and $T_{l,s}$, were fixed at 1×10^{-6}. For the full DCM, the absolute tolerance was set to $1\text{x}10^{-6}$ for all variables, except the droplet radius, which had a tolerance of $1\text{x}10^{-7}$. The tolerances were chosen to yield the fastest computation times for both models, respectively. The delumping step was performed following the solution of the DQMoM

differential equations from the initial to the final time and the numerical integration associated with delumping was performed using the trapezoid rule.

With regard to CFD simulations, in which droplet source terms feed into a CFD gas-phase solver, it would be necessary to perform delumping at every time step, rather than solving the DQMoM equations for the entire time interval and subsequently delumping all times at once. It is emphasized that despite the fact that the integrals in Eqs. (32) and (33) are "history" integrals from 0 to t, within a CFD simulation it would not be necessary to store the values of B_M, A, C, D_i and E_i at all times, which could become memory intensive. Rather, when performing delumping following every DQMoM time step, the integrals from 0 to t are broken into two parts. Using the integral in Eq. (32) as an example:

$$(36)\ \int_0^t -ACln(1+B_M)E_i dt = \int_0^{t-\Delta t} -ACln(1+B_M)E_i dt + \int_{t-\Delta t}^t -ACln(1+B_M)E_i dt$$

The value of the first integral on the right-hand side, from 0 to $t - \Delta t$, is saved from the previous time step, and the second integral on the right hand side is evaluated using the trapezoid rule, which only requires values at the current and previous time step. For the integral in Eq. (36), this can be written as

$$(37)\ J_i(t) = J_i(t-\Delta t) + \frac{\Delta t}{2}[p_i(t-\Delta t) + p_i(t)]$$

where the integral and integrand are represented by J_i and p_i, respectively,

$$(38a)\ J_i(t) \equiv \int_0^t -ACln(1+B_M)E_i dt$$

$$(38b)\ p_i(t) \equiv -ACln(1+B_M)E_i$$

Therefore, using the trapezoid rule, which is second order accurate, only data from the most recent time step, such as $J_i(t-\Delta t)$ and $p_i(t-\Delta t)$ needs to be saved, despite the fact that the limits of integration are from 0 to t. If higher order is desired in the delumping integrals, which does not seem necessary based on the results presented in Section 3, data from one or two more previous steps could be saved, but in no situation would the entire history from 0 to t

be required. Following the delumping step, the updated values of J_i and p_i replace the old values and are saved for the next time step. As mentioned above, for the results presented in Section 3, DQMoM was solved for the entire interval, followed by delumping the results for all times. However, a separate MATLAB code was written and tested which verified the success of the procedure outlined above for performing delumping at every time step with only a small difference in computational expense, as discussed in Section 3.2.

3. Results and discussion

From a continuous thermodynamics perspective, a full discrete component model, such as Eq. (6), is an exact solution. Therefore, DQMoM with delumping has been tested by comparison to the full DCM. The fidelity with which DQMoM captures the evolution of the mixture as a whole largely determines the accuracy of the overall approach, since the delumping step is exact, with the exception of error from the numerical integration of Eqs. (32) and (33). The physical properties for the discrete species in the full DCM have been calculated using the same correlations with normal boiling point as used in DQMoM with delumping.[31]

3.1. Test case #1: droplet composed of 36 species

The first test case is similar to that of Laurent and coworkers:[15,20] a kerosene droplet, initially at 300 K, comprised of 36 components[20] with an initial diameter of 50 μm, vaporizing in an environment at 500 K and 500 kPa. Fig. 1 shows the initial droplet composition, which was taken to be identical to that given by Laurent.[31] The mole fraction distribution exhibits several local peaks and may not be amenable to treatment with a standard prescribed distribution function, such as a gamma function. The far-field composition, on a molar basis, is 70% air and 30% isohexane, the latter being the droplet component with the lowest normal boiling point. Laurent et al. point out that the case of a single volatile component present at the far-field boundary is a difficult test-case for CTM methods.[20] Although Laurent et al.[20] and Bruyat et al.[15] do not provide the equations used to compute the droplet temperature and radius, the equations used in this study are taken from the earlier

thesis of Laurent[31] and are given in Appendix B. It is also noted that in this study, the vapor boundary conditions, $x^i_{g,\infty}$, are taken to be constant, similar to Bruyat et al.[15] For both the full DCM and DQMoM with delumping, the internal temperature gradients and the evolution of droplet radius are calculated in the same manner.

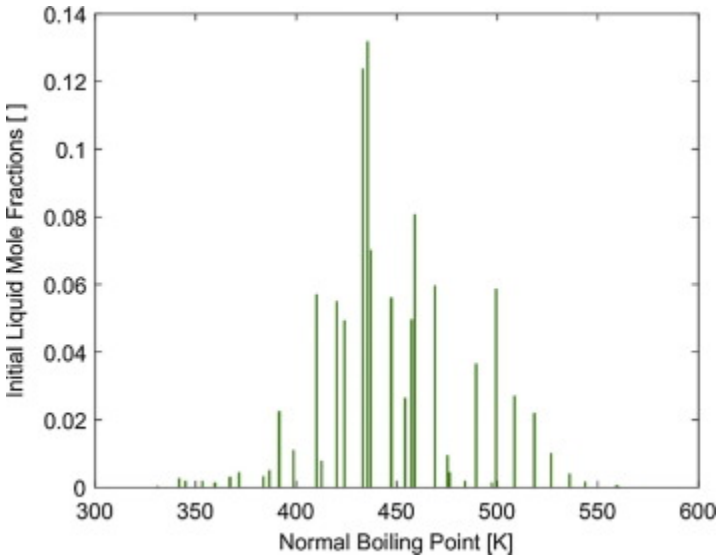

Fig. 1. Initial discrete liquid mole fraction distribution for a kerosene droplet [20].

The high accuracy of Gaussian quadrature compared to other interpolation formulas is only realized if the function within the integrand, $f(I)$, which multiplies the weight function, $x_l(I)$, is sufficiently smooth and could be approximated by a polynomial. Comparing Eqs. (12) and (21) and factoring out constant terms with respect to it is seen that in this case, the function, is given by

$$(39)\ f(I) = I^k[1 - \frac{P_{sat}(I)}{P_\infty}\left(1 + \frac{1}{B_M}\right)]$$

Fig. 2 shows this function evaluated at three distinct times, for k = 1, 2, for the test case described above. Fig. 2 confirms that $f(I)$ is smooth and well approximated by a polynomial and therefore the quadrature approximation at the heart of DQMoM is appropriate in this case.

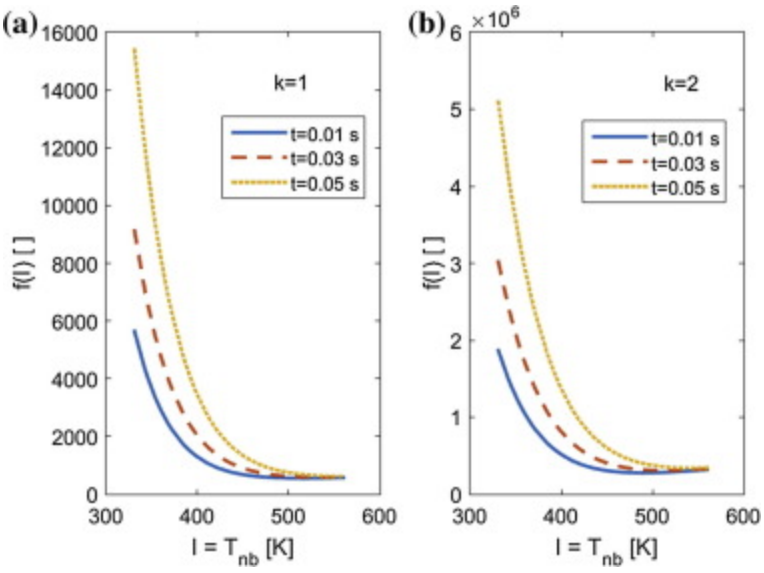

Fig. 2. Integrand function, $f(I)$, for the Gaussian quadrature for (a) k = 1 and (b) k = 2, at three times.

Using QMoM or DQMoM alone can provide information on the behavior of the droplet as a whole, while the delumping step provides information on the behavior of individual species. Fig. 3 shows the evolution of the weights, w_j, and nodes, I_j, for DQMoM with delumping for three cases: N = 2, 3, 4.

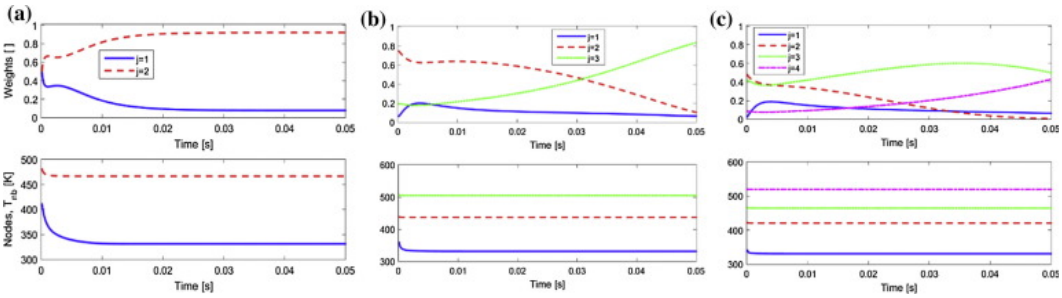

Fig. 3. Evolution of the weights (top) and nodes (bottom) for (a) N = 2, (b) N = 3 and (c) N = 4, as calculated by DQMoM.

Similar to the results of Bruyat et al. it is observed that the weights and nodes are well-behaved in DQMoM, in contrast to the erratic behavior of the nodes and weights observed for QMoM in some cases.[15] It is also seen that the weights repeatedly intersect one another and this occurred without numerical difficulties.

Fig. 4 compares the performance of DQMoM with delumping to the full DCM solution for the calculation of the total molar vapor flow rate from the droplet, $\dot{n}^{tot}$. The initial flow rate is negative, which implies that vapor is condensing onto the droplet due mostly to the initially low droplet temperature. After the temperature increases and vaporization begins to dominate condensation, the net flow rate becomes positive. It is observed that using DQMoM with N = 2 nodes yields results that differ from the exact (DCM) solution, but DQMoM with both N = 3 and N = 4 produces very good agreement.

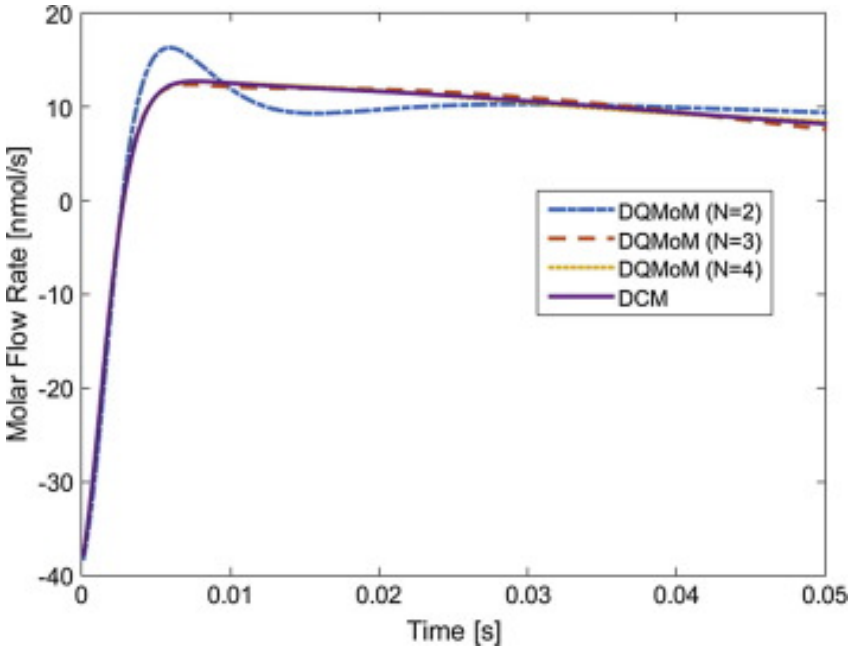

Fig. 4. Evolution of total molar flow rate with time for DQMoM (N = 2, 3 and 4) and the full DCM.

Fig. 5 compares the mean normal boiling point calculated using DQMoM with delumping to that calculated using the full DCM. Consistent with Fig. 4, the mean T_{nb} initially decreases due to condensation of isohexane from the vapor-phase. Since isohexane is the component with the lowest T_{nb} (331 K), this reduces the mean boiling point of the droplet. As the droplet temperature increases, the mean normal boiling point starts to increase, as vaporization begins to dominate condensation and the lighter components preferentially vaporize and leave behind components with higher boiling points. Again, DQMoM with N = 2 nodes yields results that differ from the

exact (DCM) solution, but DQMoM with both N = 3 and N = 4 produces good agreement.

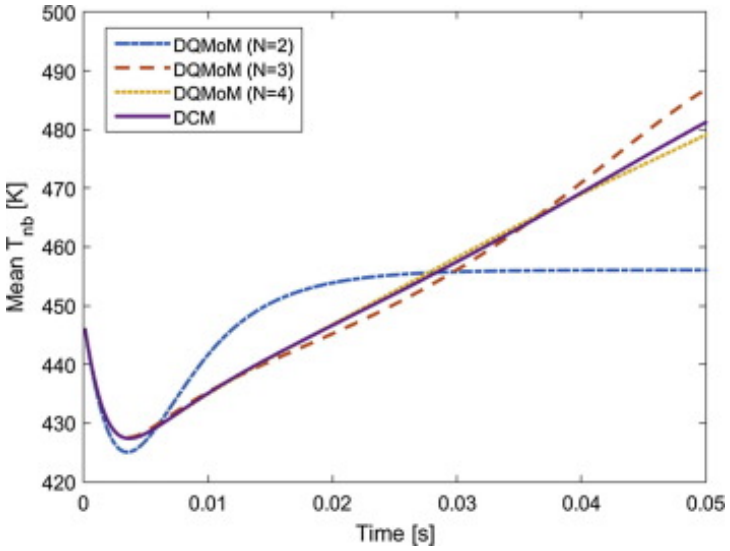

Fig. 5. Evolution of mean normal boiling point of the droplet with time for DQMoM (N = 2, 3 and 4) and the full DCM.

Results for other variables associated with the droplet as a whole, such as the evolution of droplet radius, mean temperature and surface temperature (not shown) also indicate that DQMoM with N = 3 or N = 4 produces excellent agreement with the full DCM approach, despite the droplet composition distribution being irregular. DQMoM can be used to predict the evolution of global variables associated with the mixture and droplet as a whole, which is in agreement with the conclusion reached by Laurent, Bruyat and coworkers.[9,15,20]

The novelty of the present work is the delumping step that is appended to DQMoM and which can provide significantly more information with a minimal increase in the computational cost. Fig. 6 demonstrates this capability of DQMoM with delumping (N = 3) to the exact DCM solution at three different times. The agreement is excellent, although only six differential equations, three for w_j and three for $(w_j I_j)$, are solved for the species equation using DQMoM with delumping (Eq. (20)), compared with 36 for full DCM (Eq (6)). Due to the addition of the delumping step,

DQMoM is able to provide the same information as the full DCM, with excellent accuracy, while solving many fewer ODEs.

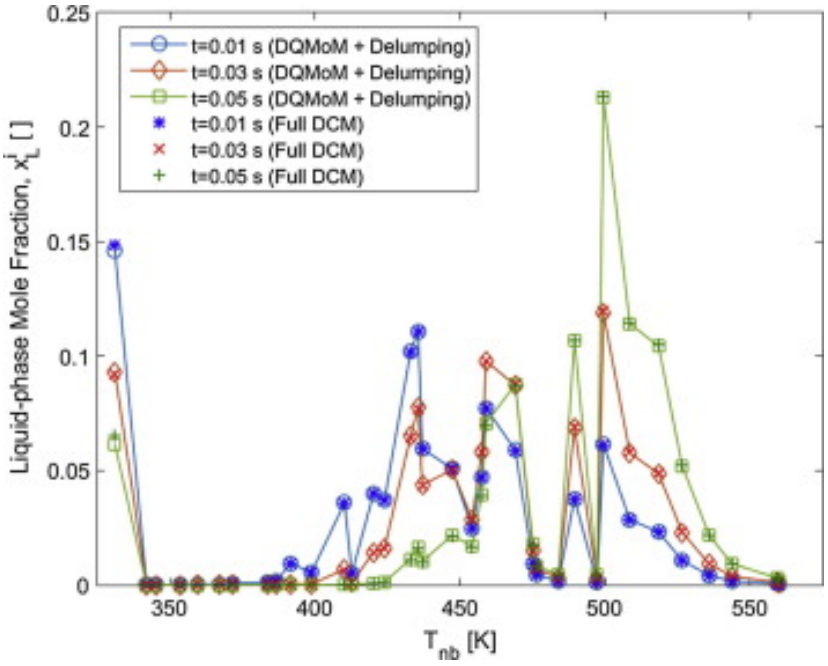

Fig. 6. Comparison of liquid mole fraction distributions for all discrete species calculated using DQMoM with delumping (N = 3) and calculated using the full discrete model, at three times.

Fig. 7 shows the gas-phase mole fractions at the droplet surface for every species calculated using DQMoM with delumping (N = 3) and using the full DCM solution at the same three times. The agreement is again quite good, although there is some discrepancy at 0.05 s between the delumped solution and the full DCM for the lightest component (isohexane), which is the fuel component present at the far-field boundary.

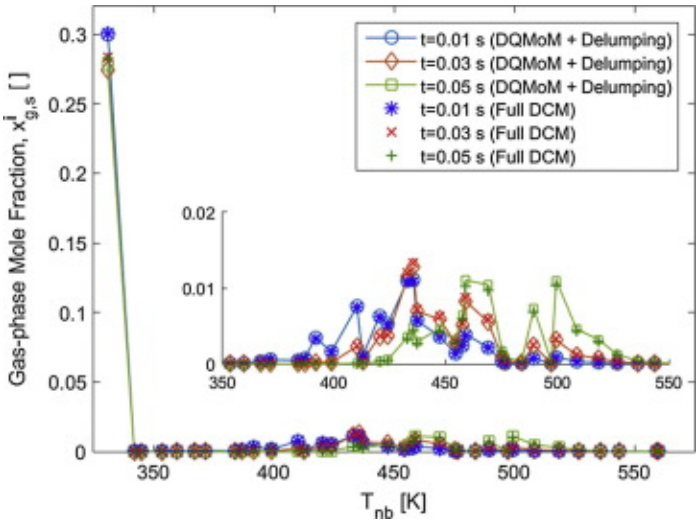

Fig. 7. Comparison of vapor mole fraction distributions for all discrete species calculated using DQMoM with delumping (N = 3) and calculated using the full discrete model, at three times. Inset: magnification of species other than isohexane (species with T_{nb} > 331 K).

In a CFD simulation, the droplets act as sources/sinks of mass and energy to the gas-phase equations. Therefore, a relevant quantity to test the performance of DQMoM with delumping compared to the full DCM solution would be the molar flux of every individual species, $\dot{n}^i$ (Eq. (7)), to or from the droplet. Furthermore, this quantity provides a good test for DQMoM with delumping since it combines the global variable, $\dot{n}^{tot}$, with the individual species mole fractions, which are calculated from the delumping step. Fig. 8a shows the individual molar fluxes for all 36 species calculated using DQMoM with delumping (using N = 3) and using the full DCM solution at the same three times, as well as an earlier time (0.0034 s) when condensation is apparent.

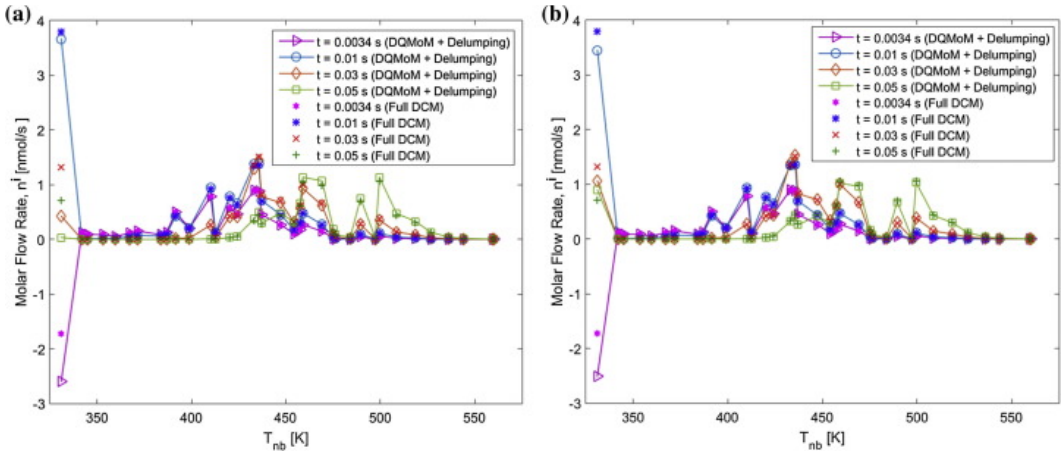

Fig. 8. Comparison of molar flow rates for all discrete species calculated using DQMoM with delumping and calculated using the full discrete model, at three times, for (a) N = 3, and (b) N = 4.

It is observed from Fig. 8a that at 0.0034 s the negative total flow rate (see Fig. 4) is exclusively due to the condensation of isohexane (T_{nb} = 331 K), since it is the only species present at the far-field boundary. Furthermore, at all times, the results from DQMoM with delumping are quite accurate for every species, with the exception of isohexane, which is particularly inaccurate at the latest time.

The decrease in accuracy at later times is partly attributable to the divergence between the total molar flow rate using DQMoM with N = 3 from the full DCM solution at later times (see Fig. 4), as well as the discrepancy for gas-phase isohexane at 0.05 s (see Fig. 7). If increased accuracy in this species is required, the order of the quadrature approximation can be increased from three to four, as Fig. 4 indicates near perfect agreement in the total molar flow rate between DQMoM with N = 4 and the full DCM. Fig. 8b shows the individual molar fluxes for all 36 species calculated using DQMoM with delumping using N = 4. At 0.03 and 0.05 s the agreement for isohexane is improved and the agreement for other species is now excellent.

The decrease in computational time (wall clock) using DQMoM with delumping compared to the full DCM was 45% (N = 2), 26% (N = 3) and 28% (N = 4). The delumping step is associated with less than 2% of the total computational cost of DQMoM with delumping.

Bruyat et al. report a decrease of "at least 60%" for N = 2 and 3, for the case of constant far-field boundary conditions.[15] The reasons for the discrepancy are not clear, but it should be kept in mind that the equations solved for the droplet temperature may not be identical to those of Bruyat et al.,[15] and may be computationally more difficult. Specifically, the computational overhead associated with solving differential–algebraic equations for $\bar{T}_l$, $T_{l,s}$ and R, in the present case likely reduces the advantage of DQMoM compared to the full DCM model. It is not clear how these variables were treated by Bruyat et al.[15] Differences in the ODE/DAE solvers employed could also contribute to the difference in computational time reported here and by Bruyat and coworkers.[15] The salient point, however, is that while delumping is associated with less than 2% of the total computational cost, it enables DQMoM to provide the same information as the full DCM. For the test case described in Section 3.2 it will be seen that the efficiency of DQMoM with delumping is far superior to full DCM.

3.2. Test case #2: droplet composed of 200 species

To further illustrate the potential of DQMoM with delumping, the droplet composition was changed to include 200 hypothetical species with boiling points evenly spaced between 331 K and 560 K, with initial compositions, $x^i{}_l$, randomly assigned. Similarly, the far-field boundary conditions for vapor mole fractions of fuel, $x^i{}_{g,\infty}$, have been randomly generated for a total of 5% fuel and 95% air at the boundary. Other parameters are the same as Test case #1. The initial liquid mole fraction distribution is shown in Fig. 9a, and the constant vapor mole fraction distribution at the far-field boundary is shown in Fig. 9b.

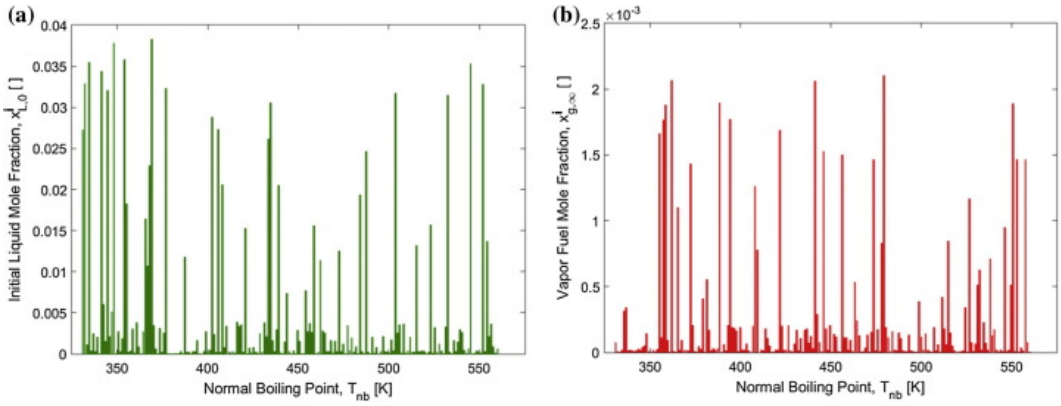

Fig. 9. (a) Initial discrete liquid mole fraction distribution for hypothetical droplet with 200 components and (b) constant vapor mole fraction distribution at the far-field boundary.

Figs. 10–12 illustrate the capability of DQMoM with delumping to accurately predict the detailed behavior of a vaporizing multicomponent droplet at a fraction of the computational cost of full discrete models. Fig. 10 shows the liquid mole fractions for all 200 components calculated using DQMoM with delumping (using N = 3) as well as the exact DCM solution at three different times. The agreement is generally excellent. It is noted that at earlier times the droplet's composition consists of both low and high boiling point species, while at later times, after the droplet temperature has increased, the composition is shifted to species with higher boiling points, as the lower boiling point species vaporize earlier and at lower temperatures.

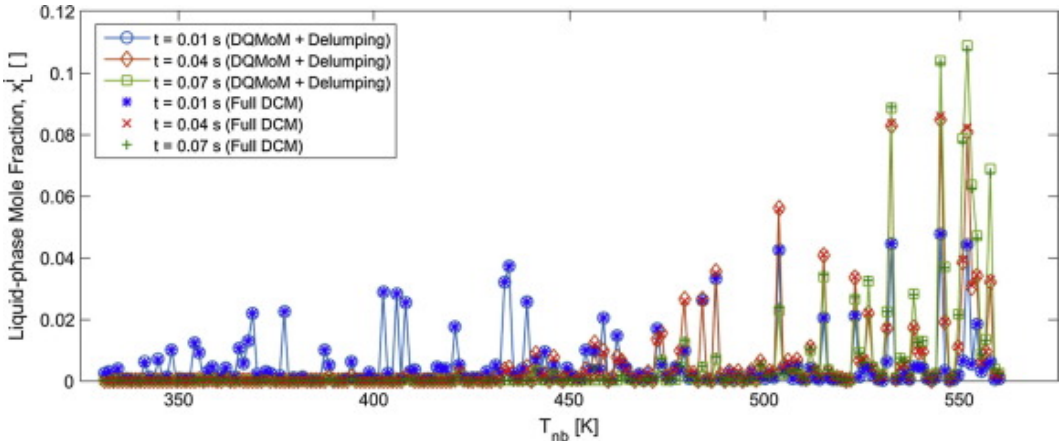

Fig. 10. Comparison of liquid mole fraction distributions for all discrete species calculated using DQMoM with delumping (N = 3) and calculated using the full discrete model, at three times.

Fig. 11 shows the gas-phase mole fractions at the droplet surface for all 200 species calculated using DQMoM with delumping (using N = 3) and using the full DCM solution at the same three times. The agreement is good, although the discrepancies that exist tend to be more prominent at later times.

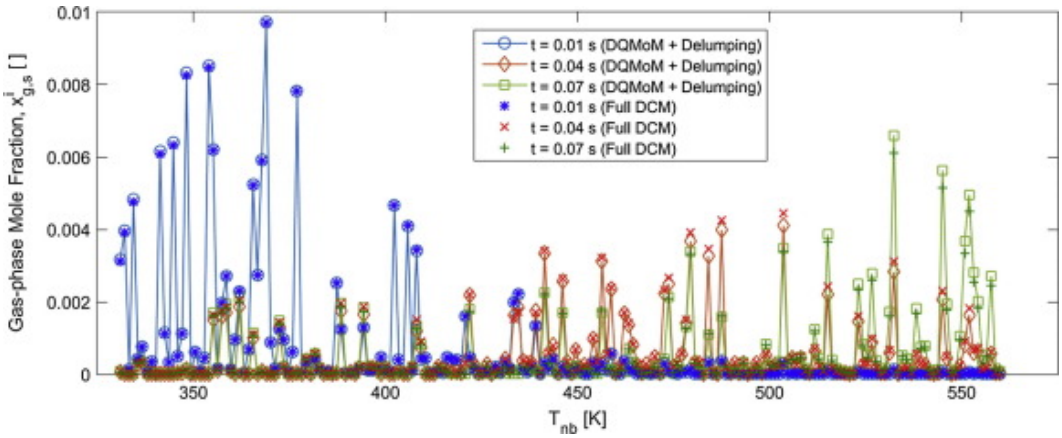

Fig. 11. Comparison of vapor mole fraction distributions for all discrete species calculated using DQMoM with delumping (N = 3) and calculated using the full discrete model, at three times.

Fig. 12a shows the molar fluxes for all 200 species calculated using DQMoM with delumping and using the full DCM solution at the same three times for N = 3. The agreement between the methods is quite good, which is especially significant given that the molar flow rates are the variables that would be important to detailed chemical kinetic mechanisms within CFD simulations. It is observed that at 0.01 s, there is vaporization of lower boiling point species from the droplet (positive flow rate) while there is condensation of higher boiling point species onto the droplet (negative flow rate). By 0.04 s the majority of the species are vaporizing rather than condensing, although there are exceptions among the species with T_{nb} > 515 K. At 0.07 s, it appears that all species with boiling points below 450 K have completely vaporized (Fig. 10) and that the significant source of vaporization lies in species with T_{nb} > 475 K.

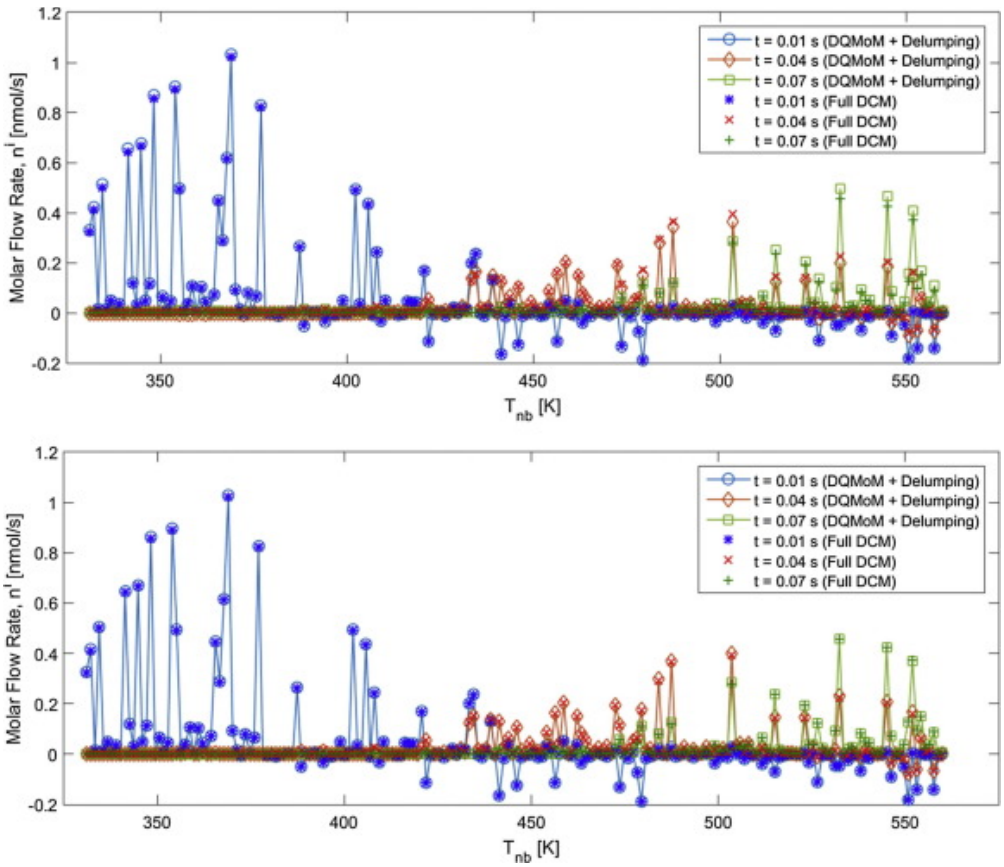

Fig. 12. Comparison of molar flow rates for all discrete species calculated using DQMoM with delumping and calculated using the full discrete model, at three times, (a) N = 3 and (b) N = 4.

Some error is apparent in Figs. 11 and 12a at later times among higher boiling point species. This error can largely be removed by increasing the order of the quadrature from three to four. Fig. 12b shows the molar fluxes for all 200 species calculated using DQMoM with delumping and using the full DCM solution at the same three times for N = 4. It is observed that for all species and all times, the agreement is now excellent.

To make the comparison quantitative, the relative error in the individual molar flow rates (from Fig. 12) calculated by DQMoM with delumping (N = 3) is shown in Fig. 13a for species with absolute flow rates in excess of 0.15 nmol/s. At the 0.01 s, the relative error is roughly 2% or less for all species above the cutoff flow rate, while at 0.04 s and 0.07 s, all species have relative errors smaller than 12%.

Increasing the number of DQMoM nodes to N = 4 reduces the errors to less than 4% for all the species above the cutoff, even at the latest time, which can be seen in Fig. 13b. Most species have errors of less than 2%. This level of accuracy has been achieved solving only eight differential equations for the species distribution rather than the 200 that are associated with the full DCM.

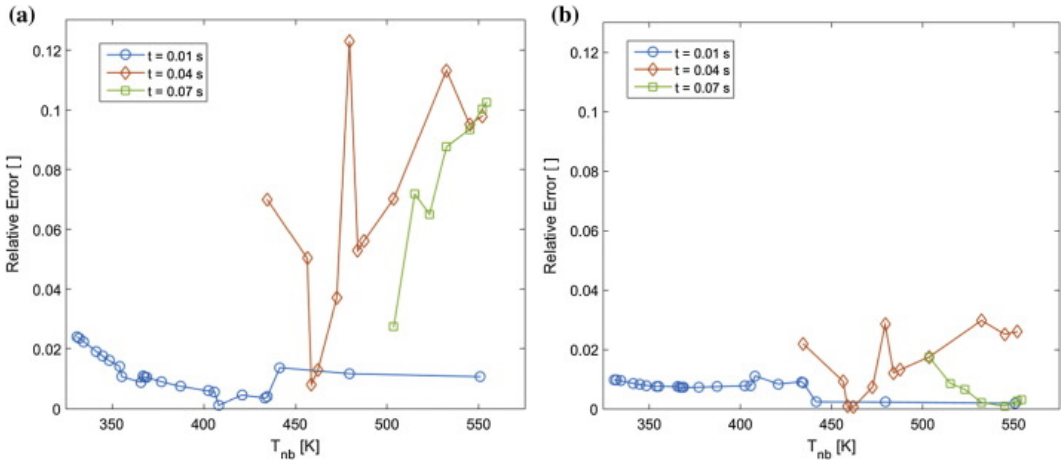

Fig. 13. Relative error in molar flow rates calculated using DQMoM with delumping. (a) N = 3; (a) N = 4.

In Fig. 14, the computational performance of DQMoM with delumping (N = 2, 3, 4) is compared to the full DCM in terms of wall-clock time for 50, 100 and 200 randomly generated species for the same test case. The solution is calculated up to 0.09 s. The cost of integrating the governing differential equations is shown by the solid bar and the cost of the delumping step (for DQMoM) is shown by the white upper bars.

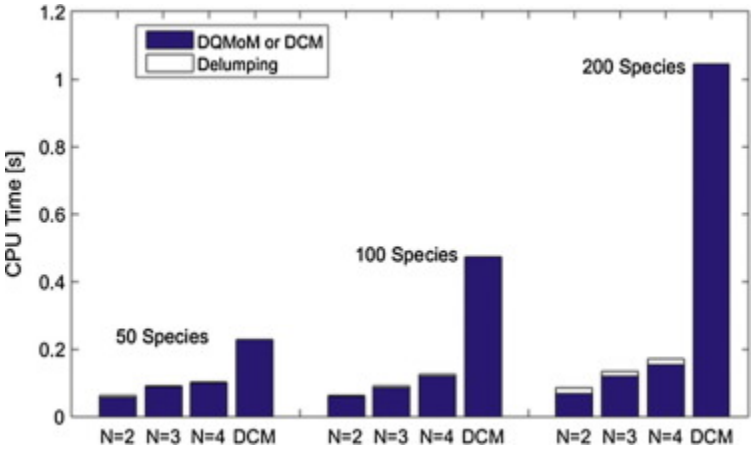

Fig. 14. Computation time as a function of modeling approach and number of species.

It can be seen that the computational cost of the delumping procedure is quite small compared to solving the governing differential equations of DQMoM. This is to be expected, since the delumping step only requires numerical integration of existing data. It is also observed that as the number of species increases, the benefit of using DQMoM with delumping compared to full DCM increases, since the number of differential equations to be solved using DQMoM does not increase with the number of species in the droplet, for a given *N*. Comparing DQMoM with delumping using *N* = 3, which has been shown above to be quite accurate, to the full DCM, the computational savings is 60% for 50 species, 81% for 100 species and 87% for 200 species.

As mentioned above, the results in Section 3 were obtained by solving the DQMoM equations for the entire time interval and subsequently delumping the entire solution at once, although delumping following every time step is more appropriate for implementation within CFD simulations. A code was written using the latter approach, and DQMoM with delumping exhibited the same good agreement to the full DCM, as expected. The computational savings using DQMoM with delumping following every time step (*N* = 3) compared to full DCM was 37% for 50 species, 63% for 100 species and 77% for 200 species. Finally, it is pointed out that without the computational overhead associated with solving a differential–algebraic system for $\bar{T}_l$, $T_{l,s}$ and *R*, the substantial advantage of DQMoM with delumping compared to full DCM would likely be even greater.

4. Conclusions

A delumping procedure has been developed and paired with the Direct Quadrature Method of Moments to simulate the vaporization of multicomponent droplets. DQMoM with delumping generates the detailed species information associated with discrete component models at the computational cost of continuous thermodynamic models. The delumping procedure can be combined with any continuous thermodynamic approach, with the only restriction being that the nonlinearity in the corresponding discrete species equation appears exclusively in terms associated with the multicomponent mixture as whole. Since these terms can be approximated accurately

using the CTM solution, the discrete species equation can be converted into a linear, first order differential equation with an exact solution in terms of numerically evaluated integrals.

Although DQMoM with delumping has been applied in this study to a well-mixed droplet, similar to that studied by Laurent and coworkers,[9,15,20] this is not a fundamental restriction associated with continuous thermodynamic approaches (see e.g.[25]) or the delumping procedure. Future applications of DQMoM with delumping to droplet models with a quasi-steady parabolic species profile appear to be possible, since the nonlinearity in the governing ODE for mean mole or mass fractions can be removed by DQMoM, since it appears in terms associated with the mixture as a whole.[2] The recent power-law model, in which species profiles within the droplet transition from an initial power greater than two to quasi-steady profiles with a power of two (parabolic) via exponential decay, is interesting.[2] During the initial transient, the differential equations for mean mass fraction have nonlinearity in the mean mass fraction itself, which cannot be removed by DQMoM, rendering delumping inapplicable. However, during the exponential decay to the quasi-steady state, as well as in the quasi-steady state itself, it appears that DQMoM with delumping would be feasible.

In this study, DQMoM with delumping was applied to a kerosene droplet comprised of 36 components with the same initial composition and property relations as studied by Laurent et al.,[20] and to a hypothetical droplet consisting of 200 species with random initial liquid and far-field vapor compositions. Using only three nodes, the accuracy of DQMoM with delumping is very good in both cases, both for global variables characteristic of the droplet as a whole, as well as for the mole fractions and fluxes of individual discrete species. Computation times were reduced by 87% compared to the full DCM for the case of 200 species, while providing the same information on every discrete species.

DQMoM with delumping has good potential for implementation in CFD simulations and would enable the use of detailed gas-phase kinetic mechanisms without overburdening the simulation with dozens or hundreds of discrete differential equations for each droplet that is tracked. In a CFD simulation the vapor boundary conditions for the

droplets, $x^i{}_{g,\infty}$, would be functions of time, but this should not present a problem for the method. When the delumping is performed at every time step, as it would be in a CFD simulation, the efficiency of DQMoM with delumping is still quite good, with a reduction in CPU time of 77% compared to the full DCM for 200 species.

Acknowledgment

The author would like to thank Prof. Bill Green of the Department of Chemical Engineering at MIT for suggesting the study of multicomponent droplet vaporization.

Appendix A. Thermo-physical properties

Property correlations for kerosene components (pseudo-components or discrete components) as a function of the normal boiling point, T_{nb}, are identical to those used by Laurent et al.[20] Mixing rules that are used to obtain properties of the liquid (subscript *l*) and gas (subscript *g*) mixtures as a whole are taken from the thesis of Laurent[31] and are thought to be the same as those used by Laurent et al.[20] and Bruyat et al.[15] These mixing rules are given in terms of various moments, which are defined below for the DQMoM. In this study, kerosene is assumed to be composed of a single group (chemical family) and therefore the liquid phase consists of a single group. This assumption could be relaxed to allow for cases in which more than one group of species is present,[15,31] as mentioned above. For the gas phase, due to the presence of air, mixing rules are used to account for the existence of two groups.

A.1. Moments used in mixing rules

A.1.1. Kerosene

(A.1) $0th\ moment\ of\ liquid-phase: m^0{}_l = \sum_j w_j = 1$

(A.2) $1st\ moment\ of\ liquid-phase:\ m^1{}_l = \sum_j w_j I_j$

(A.3) $2nd\ moment\ of\ liquid-phase: m^2{}_l = \sum_j w_j I^2{}_j$

(A.4) $0th\ moment\ of\ kerosene\ in\ gas-phase\ at\ droplet\ surface: m^0{}_{g,s} = \sum_j w_{g,j}$

(A.5) $1st\ moment\ of\ kerosene\ in\ gas-phase\ at\ droplet\ surface: m^1{}_{g,s} = \sum_j w_{g,j} I_j$

(A.6) $0th\ moment\ of\ kerosene\ in\ gas-phase\ at\ far-field\ boundary: m^0{}_{g,\infty} = \sum_i x^i{}_{g,\infty}$

(A.7) $1st\ moment\ of\ kerosene\ in\ gas-phase\ at\ far-field\ boundary: m^1{}_{g,\infty} = \sum_i x^i{}_{g,\infty} I_i$

Note that $w_{g,j} = w_j \frac{P_{sat}(I_j)}{P_\infty}$ and $x^i{}_{g,\infty}$ is the gas-phase mole fraction boundary conditions.

The reference moments for the properties of the gas-phase are calculated using the 1/3 rule.

(A.8) $0th\ moment\ of\ kerosene\ in\ gas-phase\ (reference\ value): m^0{}_{g,ref} = {}^2\!/_{3m^0{}_{g,s}} + {}^1\!/_{3m^0{}_{g,\infty}}$

(A.9) $1st\ moment\ of\ kerosene\ in\ gas-phase\ (reference\ value): m^1{}_{g,ref} = {}^2\!/_{3m^1{}_{g,ref}} + {}^1\!/_{3m^1{}_{g,\infty}}$

A.1.2. Air

(A.10) $0th\ moment\ of\ air\ in\ gas-phase\ at\ surface: m^0{}_{air,s} = 1 - \sum_j w_{g,j}$

(A.11) $0th\ moment\ of\ air\ in\ gas-phase\ at\ far-field\ boundary: m^0{}_{air,\infty} = 1 - \sum_i x^i{}_{g,\infty}$

(A.12) $0th\ moment\ of\ air\ in\ gas-phase\ (reference\ value): m^0{}_{air,ref} = {}^2\!/_{3m^0{}_{air,s}} + {}^1\!/_{3m^0{}_{air,\infty}}$

A.2. Properties of Kerosene Components and Properties of Liquid and Gas-Phase Mixtures

The correlations for properties as a function of normal boiling point, $I = T_{nb}$, are given below, e.g. $P_{sat}(I)$, $MW(I)$. Most properties, such as molar mass, *MW,* are also defined for the gas and liquid mixtures as a whole, and such properties, calculated by various mixing rules, are indicated by a subscript *g* or *l*, respectively. Because only a single group is present within the droplet, certain properties of the liquid mixture as a whole, such as k_l, are simplified. Due to the mixing rules used for certain gas-phase properties, such as thermal conductivity, k_g, mixture properties for the two groups (kerosene and air) are computed as intermediates and are indicated by subscripts *ker* and *air*, respectively. Some properties, such as P_{sat}, are not required for the mixture as a whole. Finally, some mixture properties, such as the latent heat

of vaporization, I_v, are calculated as weighted averages of the molar fluxes from the droplet [31].

A.2.1. Liquid properties

Saturation vapor pressure (Pa)

$$\text{(A.13)}\ P_{sat}(I) = P_\infty \exp\left[\frac{A_0+A_1 I}{\bar{R}}\left(\frac{1}{I}-\frac{1}{T_{l,s}}\right)\right] \qquad A_0 = -3.7607 \times 10^6, A_1 = 9.4865 \times 10^4, \bar{R} = 8314\ {}^{J}/_{kmol\ K}$$

Liquid molar mass (kg/kmol)

$$\text{(A.14)}\ MW(I) = A_0 + A_1 I$$
$$MW_l = A_0 {m^0}_l + A_1 {m^1}_l$$
$$A_0 = -123.6,\ A_1 = 0.6247$$

Liquid concentration (kmol/m^3)

$$\text{(A.15)}\ C_l(I) = A_0 + A_1 I + A_2 I^2 + (B_0 + B_1 I + B_2 I^2)\bar{T}_l$$
$$C_l = A_0 {m^0}_l + A_1 {m^1}_l + A_2 {m^2}_l + (B_0 {m^0}_l + B_1 {m^1}_l + B_2 {m^2}_l)\bar{T}_l$$
$$A_0 = 4.2163 \times 10^1, A_1 = -1.3445 \times 10^{-1}, A_2 = 1.2442 \times 10^{-4}$$
$$B_0 = -7.1106 \times 10^{-2},\ B_1 = 2.5921 \times 10^{-4}, B_2 = -2.5284 \times 10^{-7}$$

Liquid heat capacity (J/kmol K)

$$\text{(A.16)}\ c_{p,l}(I) = (A_0 + A_1 I) + (B_0 + B_1 I)\bar{T}_l$$
$$c_{p,l} = (A_0 {m^0}_l + A_1 {m^1}_l) + (B_0 {m^0}_l + B_1 {m^1}_l)\bar{T}_l$$
$$A_0 = -2.2873 \times 10^5,\ A_1 = 8.2549 \times 10^2$$
$$B_0 = -7.8088 \times 10^1, B_1 = 1.6086 \times 10^0$$

Liquid thermal conductivity (W/m K)

$$\text{(A.17)}\ k_l(I) = (A_0 + A_1 I) + (B_0 + B_1 I)\bar{T}_l + (C_0 + C_1 I){\bar{T}^2}_l$$
$$k_l = (A_0 {m^0}_l + A_1 {m^1}_l) + (B_0 {m^0}_l + B_1 {m^1}_l)\bar{T}_l + (C_0 {m^0}_l + C_1 {m^1}_l){\bar{T}^2}_l$$
$$A_0 = 5.355 \times 10^{-2}, A_1 = 5.0987 \times 10^{-4}, B_0 = -2.5251 \times 10^{-4}, B_1 = -7.9625 \times 10^{-7}, C_0 = 2.483 \times 10^{-7}, C_1 = 3.2996 \times 10^{-10}$$

A.2.2. Gas properties

Gas temperature (reference) (K)

$$\text{(A.18)}\ T_g = {}^{2}/_{3T_s} + {}^{1}/_{3T_\infty}$$

[International Journal of Heat and Mass Transfer, Vol 103 (December 2016): pg. 940-954. DOI.

Gas concentration (kmol/m^3)

$$(A.19)\ C_g = \frac{P_\infty MW_g}{\bar{R}T_g} \text{ where } \bar{R} = 8314\ {}^{J}/_{kmol\ K} \text{ and } P_\infty \text{ is in } Pa$$

Gas density (kg/m^3)

$$(A.20)\ P_g = \frac{P_\infty MW_g}{\bar{R}T_g} \text{ where } \bar{R} = 8314\ {}^{J}/_{kmol\ K} \text{ and } P_\infty \text{ is in } Pa$$

Molar mass (kg/kmol)

$$(A.21)\ MW(I) = A_0 + A_1 I$$

$$MW_{g,ker} = A_0 + A_1 \frac{m^1{}_{g,ref}}{m^0{}_{g,ref}} \qquad MW_{g,air} = 28.97$$

$$MW_g = \left(A_0 m^0{}_{g,ref} + A_1 m^1{}_{g,ref}\right) + 28.97 m^0{}_{air,ref}$$

$$A_0 = -123.6, \qquad A_1 = 0.6247$$

Gas heat capacity (J/kmol K)

$$(A.22)\ c_{p,g}(I) = (A_0 + A_1 I) + (B_0 + B_1 I)T_g + (C_0 + C_1 I)T^2{}_g$$

$$c_{p,g} = \left(A_0 m^0{}_{g,ref} + A_1 m^1{}_{g,ref}\right) + \left(B_0 m^0{}_{g,ref} + B_1 m^1{}_{g,ref}\right)T_g + \left(C_0 m^0{}_{g,ref} + C_1 m^1{}_{g,ref}\right)T^2{}_g + c_{p,air} m^0{}_{air,ref}$$

$$A_0 = 1.7478 \times 10^4, A_1 = -1.0038 \times 10^1, B_0 = -8.0648 \times 10^2, B_1 = 3.8658 \times 10^0, C_0 = 3.5307 \times 10^{-1}, C_1 = -1.5673 \times 10^{-3}$$

Diffusion coefficient of kerosene in air (m^2/s)

$$(A.23)$$

$$D_g(I) = \frac{10^{-7} T_g^{1.75} \left[\frac{MW(I) + MW_{g,air}}{MW(I) MW_{g,air}}\right]^{1/2}}{P_\infty \left[(v_{g,0} + v_{g,1} I)^{1/3} + (v_g^{air})^{1/3}\right]^2} \text{ where } P_\infty \text{ is in } atm$$

$$D_g = \frac{10^{-7} T_g^{1.75} \left[\frac{MW_{g,ker} + MW_{g,air}}{MW_{g,ker} MW_{g,air}}\right]^{1/2}}{P_\infty \left[\left(v_{g,0} + v_{g,1} \frac{m^1_{g,ref}}{m^0_{g,ref}}\right)^{1/3} + (v_g^{air})^{1/3}\right]^2}$$

$$v_{g,0} = -1.7926 \times 10^2, v_{g,1} = 9.113 \times 10^{-1}, v_{g,air} = 19.7$$

Gas viscosity (kg/m s)

(A.24)

$$\mu(I) = (A_0 + A_1 I) + (B_0 + B_1 I) T_g$$

$$\mu_{g,ker} = \left(A_0 + A_1 \frac{m^1_{g,ref}}{m^0_{g,ref}}\right) + \left(B_0 + B_1 \frac{m^1_{g,ref}}{m^0_{g,ref}}\right) T_g$$

$$\mu_{g,air} = 1.13 \times 10^{-5} \sqrt{T_g}$$

$$\mu_g = \frac{m^0_{g,ref} \mu_{g,ker}}{m^0_{g,ref} \phi_{ker,ker} + m^0_{air,ref} \phi_{ker,air}} + \frac{m^0_{air,ref} \mu_{g,air}}{m^0_{g,ref} \phi_{air,ker} + m^0_{air,ref} \phi_{air,air}}$$

$$\phi_{ker,ker} = 1, \phi_{air,air} = 1$$

$$\phi_{ker,air} = \frac{\left[1 + \left(\frac{\mu_{g,ker}}{\mu_{g,air}}\right)^{\frac{1}{2}} \left(\frac{MW_{g,air}}{MW_{g,ker}}\right)^{\frac{1}{4}}\right]^2}{\left[8\left(1 + \frac{MW_{g,ker}}{MW_{g,air}}\right)\right]^{\frac{1}{2}}}$$

$$\phi_{air,ker} = \frac{\left[1 + \left(\frac{\mu_{g,air}}{\mu_{g,ker}}\right)^{\frac{1}{2}} \left(\frac{MW_{g,ker}}{MW_{g,air}}\right)^{\frac{1}{4}}\right]^2}{\left[8\left(1 + \frac{MW_{g,air}}{MW_{g,ker}}\right)\right]^{\frac{1}{2}}}$$

$$A_0 = 3.2941 \times 10^{-6}, A_1 = -4.5702 \times 10^{-9}$$

$$B_0 = 2.4177 \times 10^{-8}, B_1 = -1.9742 \times 10^{-11}$$

Gas thermal conductivity (W/m K)

(A.25)

$$k_g(I) = (A_0 + A_1 I) + (B_0 + B_1 I) T_g + (C_0 + C_1 I) T_g^2$$

$$k_{g,ker} = \left(A_0 + A_1 \frac{m^1_{g,ref}}{m^0_{g,ref}}\right) + \left(B_0 + B_1 \frac{m^1_{g,ref}}{m^0_{g,ref}}\right) T_g + \left(C_0 + C_1 \frac{m^1_{g,ref}}{m^0_{g,ref}}\right) T_g^2$$

$$k_{g,air} = 0.21\left[\frac{D_{-1}}{T_g} + D_0 + D_1 T_g + D_2 T_g^2\right] + 0.79\left[\frac{E_{-1}}{T_g} + E_0 + E_1 T_g + E_2 T_g^2\right]$$

$$k_g = \frac{m^0_{g,ref} k_{g,ker}}{1.065\left(m^0_{g,ref} \phi_{ker,ker} + m^0_{air,ref} \phi_{ker,air}\right)} + \frac{m^0_{air,ref} k_{g,air}}{1.065\left(m^0_{g,ref} \phi_{air,ker} + m^0_{air,ref} \phi_{air,air}\right)}$$

$$A_0 = -6.8725 \times 10^{-3}, A_1 = 9.8134 \times 10^{-6}$$

$$B_0 = 3.5028 \times 10^{-5}, B_1 = -6.4010 \times 10^{-8}$$

$$C_0 = 2.263 \times 10^{-7}, C_1 = -2.5570 \times 10^{-10}$$

$$D_{-1} = -3.0474 \times 10^{0}, D_0 = 1.9928 \times 10^{-2}, D_1 = 5.6861 \times 10^{-5}, D_2 = -2.2493 \times 10^{-9}$$

$$E_{-1} = -5.4318 \times 10^{0}, E_0 = 3.5487 \times 10^{-2}, E_1 = 2.6004 \times 10^{-5}, E_2 = 6.3342 \times 10^{-9}$$

Critical temperature (K)

(A.26)

$$T_{crit}(I) = A_0 + A_1 I$$
$$A_0 = 205.95, A_1 = 0.9046$$

A.2.3. Flux-weighted properties

Latent heat of vaporization (J/kmol)

(A.27)

$$l_v(I) = (A_0 + A_1 I)\left(\frac{T_{crit}(I) - T_{l,s}}{T_{crit}(I) - I}\right)^{0.38}$$

$$l_v = \sum_j \frac{\dot{N}_j l_{v,j}}{\dot{N}_{Tot}} = \left(\frac{B_M + 1}{B_M}\right)\sum_j w_{g,j}(A_0 + A_1 I_j)\left(\frac{T_{crit}(I_j) - T_{l,s}}{T_{crit}(I_j) - I_j}\right)^{0.38} - \left(\frac{1}{B_M}\right)\sum_i x^i_{g,\infty}(A_0 + A_1 I_i)\left(\frac{T_{crit}(I_i) - T_{l,s}}{T_{crit}(I_i) - I_i}\right)^{0.38}$$

$$A_0 = -3.7607 \times 10^6, A_1 = 9.4865 \times 10^4$$

Vapor heat capacity (J/kmol K)

(A.28)

$$c_{p,v} = \sum_j \frac{\dot{N}_j c_{p,g,j}}{\dot{N}_{Tot}}$$

$$c_{p,v} = \left(\frac{B_M + 1}{B_M}\right)\sum_j w_{g,j}\left[(A_0 + A_1 I_j) + (B_0 + B_1 I_j)T_g + (C_0 + C_1 I_j)T_g^2\right] - \left(\frac{1}{B_M}\right)\sum_i x^i_{g,\infty}\left[(A_0 + A_1 I_i) + (B_0 + B_1 I_i)T_g + (C_0 + C_1 I_i)T_g^2\right]$$

$$A_0 = 1.7478 \times 10^4, A_1 = -1.0038 \times 10^1$$
$$B_0 = -8.0648 \times 10^2, B_1 = 3.8658 \times 10^0$$
$$C_0 = 3.5307 \times 10^{-1}, C_1 = -1.5673 \times 10^{-3}$$

Appendix B. Models for evolution of droplet temperature and size

The applicability of DQMoM with delumping does not depend on the particular model employed for the evolution of the droplet temperature and radius. In this work, the equations used were taken from the thesis of Laurent.[31] It is not clear whether these expressions were subsequently used by Laurent et al.[20] and Bruyat et al.,[15] but it seems likely. As described in Section 2.4, a model which accounts for temperature gradients within the droplet using the parabolic assumption[22] was employed. The model solves an ordinary differential equation for the mean droplet temperature, $\bar{T}_l$,[31]

(B.1)

$$\frac{d\bar{T}_l}{dt} = \frac{3}{2}\frac{k_g Nu_g^* \ln(1 + B_T)}{C_l c_{p,l} R^2 B_T\left(1 + \frac{1}{10}\left(\frac{k_g Nu_g^* \ln(1 + B_T)}{k_l B_T}\right)\right)}\left(T_\infty - \frac{B_T l_v}{c_{p,v}} - \bar{T}_l\right)$$

This is coupled with a nonlinear equation for the droplet surface temperature, $T_{l,s}$,

$$\text{(B.2)}\ T_{l,s} = \bar{T}_l + \frac{R^2 C_l c_{p,l}}{15 k_l} \frac{d\bar{T}_l}{dt}$$

Eqs. (B.1) and (B.2) form a coupled differential–algebraic system because l_v and P_{sat} depend on $T_{l,s}$, which makes Eq. (B.2) a nonlinear algebraic equation.

The Spalding heat transfer number which appears in Eq. (B.1) is given by

$$\text{(B.3)}\ B_T = (1 + B_M)^{(D_g p_g c_{p,v})/(k_g MW_g)-1}$$

The differential equation used to account for the increase or decrease in droplet size is based on conservation of mass across the liquid–vapor interface:[26]

$$\text{(B.4)}\ \frac{dR}{dt} = -\frac{p_g D_g}{p_l} \frac{Sh_g^* \ln(1+B_M)}{2R}$$

References

[1]Y. Ra, R.D. Reitz. A vaporization model for discrete multi-component fuel sprays. Int. J. Multiph. Flow, 35 (2009), pp. 101-117

[2]G.J. Brereton. A discrete multicomponent temperature-dependent model for the evaporation of spherical droplets. Int. J. Heat Mass Transfer, 60 (2013), pp. 512-522

[3]S.S. Sazhin, A.E. Elwardany, E.M. Sazhina, M.R. Heikal. A quasi-discrete model for heating and evaporation of complex multicomponent hydrocarbon fuel droplets. Int. J. Heat Mass Transfer, 54 (2011), pp. 4325-4332

[4]S.S. Sazhin, M. Al Qubeissi, R. Nasiri, V.M. Gun'ko, A.E. Elwardany, F. Lemoine. A multi-dimensional quasi-discrete model for the analysis of Diesel fuel droplet heating and evaporation. Fuel, 129 (2014), pp. 238-266,

[5]M. Su, C.P. Chen, *et al.* Heating and evaporation of a new gasoline surrogate fuel: a discrete multicomponent modeling study. Fuel, 161 (2015), pp. 215-221

[6]R.L. Cotterman, R. Bender, J.M. Prausnitz. Phase equilibria for mixtures containing very many components. Development and application of continuous thermodynamics for chemical process design. Ind. Eng. Chem. Process Des. Dev., 24 (1985), pp. 194-203,

[7]J. Tamim, W.L.H. Hallett. A continuous thermodynamics model for multicomponent droplet vaporization. Chem. Eng. Sci., 50 (1995), pp. 2933-2942

[8]W.L.H. Hallett. A simple model for the vaporization of droplets with large numbers of components. Combust. Flame, 121 (2000), pp. 334-344

[9]C. Laurent, G. Lavergne, P. Villedieu. Continuous thermodynamics for droplet vaporization: comparison between Gamma-PDF model and QMoMC. R. Mec., 337 (2009), pp. 449-457

[10]P.L.C. Lage. The quadrature method of moments for continuous thermodynamics. Comput. Chem. Eng., 31 (2007), pp. 782-799

[11]H.M. Hulburt, S. Katz. Some problems in particle technology: a statistical mechanical formulation. Chem. Eng. Sci., 19 (1964), pp. 555-574

[12]R. McGraw. Description of aerosol dynamics by the quadrature method of moments. Aerosol Sci. Technol., 27 (1997), pp. 255-265

[13]D.E. Marchisio, R.O. Fox (Eds.), Multiphase Reacting Flows: Modeling and Simulation, Springer Wien, New York (2007)

[14]R.G. Gordon. Error bounds in equilibrium statistical mechanics. J. Math. Phys., 9 (1968), pp. 655-663

[15]A. Bruyat, C. Laurent, O. Rouzaud, Direct Quadrature Method of Moments for Multicomponent Droplet Spray Vaporization, in: 7th Int. Conf. Multiph. Flow, 2010, 8.4.3.

[16]D.L. Marchisio, R.O. Fox. Computational Models for Polydisperse Particulate and Multiphase Systems. Cambridge University Press (2013)

[17]D.L. Marchisio, R.O. Fox. Solution of population balance equations using the direct quadrature method of moments. J. Aerosol Sci., 36 (2005), pp. 43-73

[18]M. Burger, R. Schmehl, K. Prommersberger, O. Schäfer, R. Koch, S. Wittig. Droplet evaporation modeling by the distillation curve model: accounting for kerosene fuel and elevated pressures. Int. J. Heat Mass Transfer, 46 (2003), pp. 4403-4412

[19]E.M. Sazhina, S.S. Sazhin, M.R. Heikal, W.I. Babushok, R.J.R. Johns. A detailed modelling of the spray ignition process in Diesel engines. Combust. Sci. Tech., 160 (2000), pp. 317-344

[20]C. Laurent, G. Lavergne, P. Villedieu. Quadrature method of moments for modeling multi-component spray vaporization. Int. J. Multiph. Flow, 36 (2010), pp. 51-59

[21]L.A. Dombrovsky, S.S. Sazhin. A parabolic temperature profile model for heating of droplets. ASME J. Heat Transfer, 125 (2003), pp. 535-537

[22]L.A. Dombrovsky, S.S. Sazhin. A simplified non-isothermal model for droplet heating and evaporation. Int. Commun. Heat Mass Transfer, 30 (2003), pp. 787-796

[23]S.S. Sazhin, P.A. Krutitskii, W.A. Abdelghaffar, E.M. Sazhina, S.V. Mikhalovsky, S.T. Meikle. Transient heating of diesel fuel droplets. Int. J. Heat Mass Transfer, 47 (2004), pp. 3327-3340

[24]D.J. Torres, P.J. O'Rourke, A.A. Amsden. A discrete multicomponent fuel model. At. Sprays., 13 (2003), pp. 131-172

[25]Z. Abdel-Qader, W.L.H. Hallett. The role of liquid mixing in evaporation of complex multicomponent mixtures: modelling using continuous thermodynamics. Chem. Eng. Sci., 60 (2005), pp. 1629-1640

[26]B. Abramzon, W.A. Sirignano. Droplet vaporization model for spray combustion calculations. Int. J. Heat Mass Transfer, 32 (1989), pp. 1605-1618

[27]J.C. Wheeler. Modified moments and Gaussian quadratures. Rocky Mt. J. Math., 4 (1974), pp. 287-296,

[28]D.V. Nichita, C.F. Leibovici. An analytical consistent pseudo-component delumping procedure for equations of state with non-zero binary interaction parameters. Fluid Phase Equilib., 245 (2006), pp. 71-82

[29]M. Petitfrere, D.V. Nichita, F. Montel. Multiphase equilibrium calculations using the semi-continuous thermodynamics of hydrocarbon mixtures. Fluid Phase Equilib., 362 (2014), pp. 365-378

[30]C.H. Edwards, D.E. Penney. Differential Equations and Boundary Value Problems. (second ed.), Prentice-Hall, Upper Saddle River, New Jersey (2000)

[31]C. Laurent, Développement et validation de modèles d'évaporation multi-composant (Ph.D. Thesis), Universite de Toulouse, l'Institut Supérieur de l'Aéronautique et de l'Espace, 2008.

[32]N. Doué, Modélisation de l'évaporation de gouttes multi-composants (Ph.D. Thesis), L'École Nationale Supérieure, De l'Aéronautique et de l'Espace, 2005.

[33]A.C. Hindmarsh, P.N. Brown, K.E. Grant, S.L. Lee, R. Serban, D.E. Shumaker, *et al.* SUNDIALS: Suite of Nonlinear and Differential/Algebraic Equation Solvers. ACM Trans. Math. Softw., 31 (2005), pp. 363-396